Ensemble docking to difficult targets in early-stage drug discovery: Methodology and application to fibroblast growth factor 23

Hector A. Velazquez,[1,2] Demian Riccardi,[1,2] Zhousheng Xiao,[3] Leigh Darryl Quarles,[3] Charless Ryan Yates,[4] Jerome Baudry,[1,2] Jeremy C. Smith[1,2]

[1]UT/ORNL Center for Molecular Biophysics, Oak Ridge National Laboratory, Oak Ridge, TN, USA

[2]Department of Biochemistry and Cellular and Molecular Biology, University of Tennessee, Knoxville, TN, USA

[3]Department of Medicine, College of Medicine, University of Tennessee Health Science Center, Memphis, TN, USA

[4]Department of Pharmaceutical Sciences, College of Pharmacy, University of Tennessee Health Science Center, Memphis, TN, USA

Abstract:

Ensemble docking is now commonly used in early-stage in silico drug discovery and can be used to attack difficult problems such as finding lead compounds which can disrupt protein–protein interactions. We give an example of this methodology here, as applied to fibroblast growth factor 23 (FGF23), a protein hormone that is responsible for regulating phosphate homeostasis. The first small-molecule antagonists of FGF23 were recently discovered by combining ensemble docking with extensive experimental target validation data (Science Signaling, 9, 2016, ra113). Here, we provide a detailed account of how ensemble-based high-throughput virtual screening was used to identify the antagonist compounds discovered in reference (Science Signaling, 9, 2016, ra113). Moreover, we perform further calculations, redocking those antagonist compounds identified in reference (Science Signaling, 9, 2016, ra113) that performed well on drug-likeness filters, to predict possible binding regions. These predicted binding modes are rescored with the molecular mechanics Poisson–Boltzmann surface area (MM/PBSA) approach to calculate the most likely binding site. Our findings suggest that the antagonist compounds antagonize FGF23

through the disruption of protein–protein interactions between FGF23 and fibroblast growth factor receptor (FGFR).

Keywords: ensemble docking, fibroblast growth factor, MM/PBSA, molecular dynamics

Introduction

A goal of structure-based drug design is to improve the process of identifying and optimizing lead compounds against specific protein targets when compared to traditional high-throughput, brute-force experimental screening of chemical libraries to identify drug candidates by employing the use of rapidly evolving computational and experimental technologies.[1–3] For example, X-ray crystal structures have been used in conjunction with in silico virtual screening procedures to identify possible lead compounds. While this approach has been successful in several cases,[4–6] docking to crystal structures suffers from the disadvantage of not incorporating protein flexibility.[7,8]

One objection to including protein flexibility has been that modeled conformations of target proteins have performed poorly compared to apo and holo crystal structures in enrichment studies.[9] However, others have shown that incorporating protein flexibility can lead to enhanced enrichment[10,11] as well as identifying novel ligands.[12]

Treating a receptor as a rigid structure can result in potential lead compounds being missed.[13] Docking to a static crystal structure only accounts for a single binding pocket shape. For example, if only an apo crystal structure is available, a holo pocket shape that is receptive to ligand design may be difficult to discover.[9] Moreover, binding pockets of holo crystal

structures are biased toward molecular inhibitor architectures that align with the ligand of the crystal structure. Biasing ligand searches in this way can also make it difficult to find novel inhibitor scaffolds. One way to incorporate protein flexibility is to hold the ligand fixed and relax the protein around it[14] in an "induced fit mechanism." This approach can be useful in lead optimization, but suffers from the drawback that small molecules are likely to have multiple free energy minima.[15]

Conformational sampling of small molecules inside rigid binding pockets is an area that has been heavily explored to find the best ligand pose for the pocket shape that typically is found in the protein target's crystal structure. Early studies focused on using methods such as simulated annealing,[16] multiple-start Monte Carlo,[17] and genetic algorithms.[18] Other methods involve sampling low-energy Conformational spaces based on statistical mechanics[19] and tabu searches.[20] In one study examining docking algorithms, it was shown that ligand sampling methods have improved dramatically over the years.[21] However, ligand conformational sampling issues remain in docking simulations. For example, docked poses are often difficult to reproduce,[22] or their docking scores from programs may be inferior to molecular mechanics–generalized Born surface area (MM/GBSA) [23] calculations.

The above discussed challenges in computational drug discovery set the stage for the development of various flavors of ensemble docking, a promising approach that explores a variety of binding pocket shapes. Briefly, ensemble docking involves the creation of an ensemble of structures that are used for docking in an effort to incorporate protein flexibility. These methods vary in the way the ensembles are constructed, but they all seek to take into account the dynamic nature of proteins. Some approaches derive ensembles of structures from multiple X-ray crystal[14,24] or NMR structures.[25] Ensembles have also been generated from homology

models, an approach that has been found to yield better enrichment than docking to ensembles of crystal structures.[11,26,27] Indeed, homology modeling has benefited from development and refinement over the years, improving its reliability for drug discovery.[28] The increase in the number of structures available in the Protein Data Bank has made it increasingly likely that suitable structural templates can be identified for a given protein sequence for which no X-ray or NMR structure exists. Various molecular dynamics (MD) methods have also been used to create ensembles of structures for docking.[10,29]

Aiding these developments, methods to predict hot spots on a protein surface that are amenable to inhibitor binding have also been developed. For example, computational solvent mapping techniques now exist to identify parts of protein surfaces that may be amenable to fragment-based design, and these methods have been used successfully to identify binding pockets.[30–34]

Although the above methods have been developed and used independently to improve the drug design process using known systems, it remains a challenge to apply them to systems for which there is not only sparse knowledge about known inhibitors, but also very little knowledge about regions of the target that are amenable to drug design. An example of such a system is FGF23, for which only a partial crystal structure currently exists.[35]

FGF23 maintains phosphate homeostasis through protein–protein interactions with a receptor complex comprised of fibroblast growth factor receptor (FGFR) and α-klotho.[36–38] The ability to control the equilibria of protein–protein binding involved in the regulation of phosphate homeostasis is desirable not only for the advancement of general chemical knowledge of FGF23, but also for the advancement of treatments for disorders caused by excess FGF23 signaling. These include treatments for hereditary forms of hypophosphatemia[39,40] as well as adverse

cardiovascular and infectious outcomes in patients with chronic kidney diseases that are attributed to secondary elevation of FGF23.[41–48] There is therefore a need to selectively reduce the adverse effects of excess FGF23 signaling by developing inhibitors that can modulate protein–protein interactions between FGF23 and its receptor complex.

Recently, a small-molecule antagonist of FGF23 was discovered based on ensemble docking and subjected to rigorous experimental validation including co-immunoprecipitation experiments, thermal shift assays, and a dose-dependence study to assure that the compound not only disrupts formation of the FGF23:FGFR: α-klotho trimeric complex, but is selective to FGF23.[49] This antagonist was also subjected to a mouse model of hypophosphatemia, and the compound is shown to have the therapeutic potential to alleviate the disorder. Although a lack of structural information makes FGF23 a difficult protein target for rational drug design, advances that incorporate protein flexibility have made it possible to identify inhibitors.[10,50–54] In this study, we describe the successful discovery strategy for this difficult target. This strategy can in principle be applied to other "difficult" to drug protein targets. Homology modeling, ensemble docking, computational solvent mapping, and MD simulations with associated trajectory analysis were used synergistically to identify and characterize FGF23 antagonist molecules. Moreover, we perform redocking of the experimentally validated inhibitors to predict possible binding regions. These predicted binding modes are rescored with the MM/PBSA approach to calculate the most favorable binding sites. Our findings suggest that the antagonist compounds disrupt protein–protein interactions between FGF23 and FGFR.

Methods

We used a variety of computational techniques to generate a set of trial compounds, beginning with an in silico high-throughput virtual screening campaign with AutoDock Vina.[55] The results of this high-throughput screening campaign were used to suggest trial compounds that resulted in the experimentally validated FGF23 inhibitors of Xiao et al.[49] In Xiao et al., the compounds underwent target engagement tests and displayed effectiveness in treating excess FGF23 signaling in mouse model experiments. The workflow of the present study is illustrated in Scheme 1.

Two of the validated FGF23 antagonists from Xiao et al.[49] performed well on drug-likeness filters.[56–62] These two compounds were redocked in the present work with a multicenter ensemble docking (MED) protocol to propose binding regions of the drug-like compounds. The poses from the MED protocol with the best binding affinities were refined with MD simulation and MM/PBSA rescoring, resulting in a binding pocket and ligand pose that can be used for further lead optimization work. The results suggest that the ligand binds in a groove where residues are present that were predicted by Yamazaki et al.[37] to participate in protein–protein interactions with FGFR. To conduct a further computational test of Yamazaki's prediction, protein–protein docking calculations were performed to create model structures of the FGF23:FGFR1 complex and probe which FGF23 residues might engage in protein–protein contacts with FGFR1.

In silico virtual screening to identify trial compounds

Four computational models of $FGF23_{Nterm}$ were prepared. One of the models used the $FGF23_{Nterm}$ crystal structure (PDBID: 2P39),[35] and three homology models were generated with the Max Planck Bioinformatics Toolkit[63] in which an HHPred sequence search[64]

resulted in the selection of three crystal structures, two of FGF19 (PDB IDs: 1PWA[65] and 2P23[35), and one of FGF12 (PDB ID: 1Q1U[66]). These structures were used as templates to generate the homology models with Modeller.[67] These four models were subsequently refined with short, backbone-restrained molecular dynamics simulations.

All four models were prepared with charmm-gui[68] and equilibrated with charmm.[69] Hydrogen atoms were added with the HBUILD facility of charmm,[70] and each model was solvated in a periodic, octahedron solvent box ($a = b = c = 85$ Å). The energies of each structure were minimized for 500 steps of steepest descent[71] and 500 steps Adopted Basis Newton–Raphson (ABNR)[72] with the backbone and side chains restrained using 1.0 and 0.1 kcal mol^{-1} $Å^{-2}$ harmonic potentials, respectively. Using the same restraints on the solute, the solvent was relaxed by performing a short MD equilibration within the NVE ensemble for 200 ps with a 1 fs time step. For production MD simulations, the same harmonic restraint was used for the backbone, while the side chains were unrestrained. The SHAKE[73] algorithm was used to constrain all bonds to hydrogen in the solvent relaxation and production simulations. The simulations were carried out within the NPT ensemble at 298 K and 1 atm. Eight independent random seeds were used to initiate simulations for each homology model; each seed was run for 7 ns with a 2 fs time step.

The final MD configuration for each seed of each homology model was submitted to the FTMap web server[32] to identify binding sites predicted to be amenable to fragment-based design. The possible sites generated by FTMap were culled to create a reduced number of possible binding centers (at least 7.5 Å apart) using K-means clustering and HackaMol.[74] NCI Diversity Set 2 was used to carry out initial screens for the last eight snapshots of each seed for each homology model. Thus, NCI Diversity Set 2 was screened against a total of 256 $FGF23_{Nterm}$ snapshots at

each culled center. Subsequently, the ZINC Drugs Now database[75,76] was screened for molecules with a Tanimoto cutoff[77–79] of 0.8 against the same culled centers in all 256 snapshots. Open Babel[80] was used to generate the starting configuration of each molecule from its smiles representation.[81] MGLTools[82] was used to generate structure files in PDBQT format for each candidate small-molecule ligand and each $FGF23_{Nterm}$ configuration. HackaMol was used to automate all screens.[74] All screens were performed with AutoDock Vina.[55] A 20 Å cubic screening box, centered at the culled binding sites identified by FTMap, was used for each docking run. The exhaustiveness parameter in AutoDock Vina was set to 24.

Multicenter ensemble docking (MED) of FGF23 antagonists to the N-terminal fragment of FGF23

The above screening campaign led to the discovery of the inhibitors reported in Xiao et al.[49] In this work, we used the crystal structure with PDB ID 2P39 as the starting structure for additional, unrestrained 200 ns MD simulations of FGF23.[35] The system was solvated in an octahedron, periodic box consisting of 6,810 TIP3P[83] water molecules, and 3 Cl^- atoms were added to maintain electrostatic neutrality of the system. The crystallographic water molecules were retained. The protein topology file was generated with the parm99SB[84] version of the Cornell Force Field.[85] The use of amber in this portion of the protocol serves as an internal force field test between charmm[86] and amber.[84,87] The energy of the system was minimized via a two-step process. First, the entire $FGF23_{Nterm}$ structure was held fixed with a force constant of 500 kcal mol^{-1} $Å^{-2}$, while the system was minimized with 500 steps of steepest descent[71] followed by 500 steps with the conjugate gradient method.[88] In the second minimization step, the restraints on $FGF23_{Nterm}$ were removed, and 1,000 steps of steepest descent minimization were performed followed by 1,500 steps of conjugate gradient. The system was heated to 300 K while

holding the protein fixed with a force constant of 10 kcal mol^{-1} $Å^{-2}$ for 1,000 steps. Then, the restraints were released, and 1,000 MD steps were run. The shake[73] algorithm was used to constrain all bonds involving hydrogen in the simulations. A 200 ns MD run was performed from a randomly generated seed at 300 K using the NPT ensemble and a 2 fs time step. Trajectory snapshots were written every 1,000 MD steps. This procedure yielded a total of 100,000 snapshots for subsequent analysis.

The MD trajectories were subjected to a conformational cluster analysis as implemented in the ptraj software in amber12 with the hierarchical agglomerate clustering algorithm.[89] The analysis resulted in the identification of 68 clusters. One representative structure from each cluster was used as part small ensemble of structures for redocking the antagonist compounds. These representative structures and clusters were all obtained from the clustering of the 200 ns trajectory. From this small ensemble, four structures were randomly selected for binding site identification and docking of the experimentally verified drug-like compounds to $FGF23_{Nterm}$ with AutoDock Vina.[55] It was verified that these clusters were all unique through the use of pairwise RMSD of the alpha carbons against the 2P39 crystal structure. For the FGF23 homology models where other FGFs were used as the template structures, a 2 Å cutoff was used. FTMap[90,91] was used to identify potential binding sites for the drug-like compounds. To allow the docking simulations to search a large part of the protein surface for stable binding locations, the compounds were docked to each possible binding site identified by FTMap instead of docking them to a reduced number of centers as was carried out in the original in silico screening campaign. A 20 × 20 × 20 Å search box was used, and the exhaustiveness parameter in AutoDock Vina is set to 25. The docking poses were then compiled, and all the complexes

within one standard deviation of the top score were used to create a subset of complexes for further examination (Scheme 2).

MM/PBSA rescoring of the subsets examined with MED

The MM/PBSA approach allows the estimation of protein–ligand binding free energies according to the thermodynamic cycle illustrated in Scheme 3 and Equation 1, where $\Delta G_{\text{bind,solv}}$ is the free energy of ligand binding to the protein in aqueous solution, $\Delta G_{\text{bind,vac}}$ is the free energy of ligand binding to the protein in vacuum, $\Delta G_{\text{solv,complex}}$ is the solvation free energy of the ligand–protein complex, $\Delta G_{\text{solv,lig}}$ is the solvation free energy of the ligand, and $\Delta G_{\text{solv,receptor}}$ is the solvation free energy of the protein.

$$\Delta G_{\text{bind,solv}} = \Delta G_{\text{bind,vac}} + \Delta G_{\text{solv,complex}} - (\Delta G_{\text{solv,lig}} + \Delta G_{\text{solv,receptor}}) \quad (1)$$

A 2 ns MD simulation was carried out for each ligand-receptor structure resulting from the MED. The first 1,800 snapshots from the MD simulations were used for the MM/PBSA analysis, and the rest were discarded. This procedure was used to examine the neighborhood of ligand–protein poses in the immediate vicinity of the MED results. Poisson–Boltzmann calculations were carried out with the Sander module of amber12.[89] The charges for ZINC13407541 were derived from quantum mechanical calculations at the HF level of theory with the 6-31G* basis set after the geometries were optimized with B3LYP[92] and the same basis set. The quantum chemical calculations were carried out with Gaussian 09,[93] and the final electrostatic charges were derived with a RESP fit as implemented in antechamber.

Protein–protein docking

Protein–protein docking was performed to calculate structures of the $FGF23_{Nterm}$:FGFR1 complex. The crystal structures of $FGF23_{Nterm}$ and FGFR (PDB ID: 1FQ9) were submitted to the ClusPro 2.0 web server[94,95] without any restraints to guide the dockings. The ClusPro default settings were used. The default settings create models based on weighting the different terms of its potential energy function including favorable weights toward electrostatics, hydrophobic interactions, a combined van der Waals and electrostatic term, and a balanced function that does not favor one type of interaction over another. ClusPro outputs the top ten models for each weighting of its potential energy function by default. This resulted in the creation of 40 $FGF23_{Nterm}$:FGFR1 models for inspection.

Results

Targeting the N-terminal fragment of FGF23 in an in silico virtual screen

Previously, it has been shown that the C-terminal Portion of $FGF23_{FL}$ binds to α-klotho, whereas the N-terminal portion has certain binding epitopes that likely bind to FGFR[37] (Figure 1a). Unfortunately, only the N-terminal portion of $FGF23_{FL}$, that is, $FGF23_{Nterm}$, has been crystallized, suggesting that the C-terminal fragment of FGF23 may be disordered.[35] The disopred web server[96,97] was therefore used to probe $FGF23_{FL}$ for predicted regions of disorder (Figure 1b). The results indeed show that the 28 N-terminal residues of $FGF23_{FL}$ are likely to be disordered.

Residues 29 to 176, however, are likely to be structured (Figure 1b). These results also suggest that residues outside of this likely structured region are also predicted to be disordered and incorporate the C-terminal fragment of FGF23. In the FGF23 crystal structure, residues 29 to 170

are resolved, showing consistency between the disopred prediction and the failure to crystallize $FGF23_{Cterm}$.

The successful crystallization of $FGF23_{Nterm}$ (referred to simply as FGF23 hereafter) combined with Yamazaki's predictions[37] of the complex interface lay a path by which the FGF23:FGFR interface can be targeted for ligand design. To this end, four models of FGF23 were built and refined with short, MD simulations with the backbone constrained. Short MD simulations have been shown to be a good way to refine homology models.[98] Three of the homology models were generated from related FGF crystal structures as the template structures of the homology models (See Section 2). Using the crystal structures of other FGFs allows backbone diversity to be introduced into the models (Figure 2c), while retaining the core structural components that FGFs share due to their N-terminal homology.[66] Furthermore, ensemble docking to homology models has been shown to yield results that are of better quality than when the crystal structure alone is used.[26]

To identify pockets for use as the center of search boxes for in silico screening, the refined models were submitted to the FTMap[32,33] web server. FTMap has been shown to be adept at identifying druggable hot spots in proteins, particularly when used in conjunction with ensemble docking,[51,54] as in the present work. Various refined models yielded different numbers of potential binding sites, showing that the approach of generating several initial structural models takes into account a certain amount of protein flexibility (Figure 2 and Table 1).

The potential binding sites generated by FTMap were culled to a reduced number of binding centers (See Section 2). The results show areas that may be amenable to small-molecule binding that are not part of the region predicted by Yamazaki[37] to form protein–protein interactions

with FGFRs based on a pairwise sequence alignment with FGFR, but also some areas that are (Figure 2a).

These culled centers were used to cross-dock the NCI and ZINC libraries of compounds to 256 FGF23 snapshots from the MD simulations. This ensemble of 256 structures consisted of the last eight snapshots from each seed of the MD refinement of the four models. The ensemble was generated in this manner to rigorously incorporate side-chain flexibility into the in silico virtual screening campaign. The library was also docked to possible sites identified by FTMap that do not correspond to the predicted region for protein–protein interactions (Figure 2a). Docking to possible pockets that do not coincide with the predicted protein–protein interface (PPI) of Yamazaki[37] allowed alternative areas of the FGF23 surface to be explored by the compound library.

The results of the screen are shown in Figure 3. There is a general trend for compounds of higher molecular weight to have higher scores in the present screens. The tendency of virtual screening procedures to be biased toward higher molecular weights is well known.[99–101] Here, however, we report the raw scores without any renormalization, contrary to the prescriptions of others.[100] The purpose of the ensemble docking protocol implemented in this study is to test whether rigorous incorporation of protein flexibility in the form of a rather large ensemble of structures alone is sufficient to produce a reasonable hit rate. A reranking/renormalization of the results would detract from this goal. The FGF23 antagonists that were experimentally verified by Xiao et al.[49] from the NCI screen are NCI_116702 and NCI_97920 (Figure 3b). These two compounds had ranks of 4 and 6 in the NCI screen, respectively, showing that renormalization/reranking to incorporate the tendency of compounds with higher molecular weight to have higher ranks was not necessary in the current case.

In the case of the ZINC Drugs Now screen (Figure 3b), the compounds are already curated based on properties including molecular weight and the number of rotatable bonds. The purpose of screening ZINC Drugs Now was to search this subsection of chemical diversity space for possible drug-like compounds that act as FGF23 antagonists. Indeed, ZINC13407541 and ZINC01626100 were experimentally verified in Xiao et al.[49] to act as FGF23 antagonist compounds. Furthermore, ZINC13407541 was shown to have therapeutic potential in a mouse model of hypophosphatemia.[49] The ranks of ZINC13407541 and ZINC01626100 were 38 and 2, respectively, further displaying the effectiveness of the screening procedure used in this study (Figure 4).

The experimentally verified FGF23 antagonist compounds that performed well on drug-likeness filters,[56,57,60,62] ZINC13407541 and ZINC01626100 are shown in their highest scoring poses in Figure 5. ZINC13407541 was found bound to an area where FGF23:FGFR interactions are not predicted to form. The homology model in which the FGF12 crystal structure[66] (PDBID: 1Q1U) was used as the structural template produced the highest-ranking score for this compound. In contrast, the highest scoring pose for ZINC01626100 was in an area where FGF23:FGFR protein–protein interactions are predicted to form,[37] and was obtained from the in silico virtual screen using the FGF23 crystal structure (PDBID: 2P39). This result emphasizes the importance of the incorporation of protein flexibility in drug discovery, as shown by others.[7,10,14,50,52,53,102,103] If protein flexibility had not been incorporated in the form of an ensemble of structures generated from homology models, ZINC013407541 would not have been identified, as this compound was identified through the use of a homology model. Additionally, the in silico screening campaign predicts that ZINC13407541 binds to an area that

is not predicted to form protein–protein interactions with FGFR. This result highlights the need to search for multiple binding locations, as has been previously suggested.[51,104,105]

While the ensemble docking approach used for the in silico screening campaign was successful in proposing trial compounds that were experimentally validated as FGF23 antagonists[49] through assays and target engagement studies, AutoDock Vina has a relatively high standard error (which has been estimated as ~2.5 kcal/mol).[55] This casts some doubt as to whether the binding locations predicted by the in silico screening campaign are accurate. To shed light on this issue, we performed multicenter ensemble docking with the two drug-like FGF23 antagonist compounds.

Multicenter ensemble docking predicts that both of the drug-like compounds likely bind to the predicted FGF23:FGFR interface

AutoDock Vina's relatively high standard error means that deeper analysis is warranted of the possible binding sites of the active compounds. We used an ensemble approach to address this problem.

Here, unrestrained MD simulations were performed, in contrast to the backbone-restrained simulations of the original in silico virtual screen. The trajectories were then conformationally clustered to create an ensemble of 68 structures. Four of these structures (referred to as clusters A–D) were randomly selected, and the pairwise RMSD of the α carbons examined to ensure that the structures sampled different regions of conformational space (Figure 5a). Following this inspection, the structures were submitted to the FTMap[32,33] web server to identify possible binding locations. FTMap predicted different numbers of possible binding sites and different locations for each structure (Figure 5b and Table 2). The FTMap analysis of the clusters showed

that as the simulations progressed, possible sites were found to appear and disappear, highlighting the benefit of using multiple models.

Here, the potential binding sites identified by FTMap were not culled into a reduced number of possible binding centers. Rather, each possible binding site was used to define the center of a docking box in order to rigorously probe FGF23 for stable binding site locations. Interestingly, many of the potential binding sites found in the snapshots from the MD trajectories by FTMap lie along the region where FGF23:FGFR interactions are predicted to form by Yamazaki[37] (Figure 5b). Also, the pocket for ZINC13407541 in the original virtual screening campaign was identified as a potential site (Figure 5b).

The experimentally identified antagonist molecules that performed well on the drug-likeness filters were then docked to each possible binding site identified by FTMap. To perform these dockings, the potential binding sites identified by FTMap were used as the centers of 20 × 20 × 20 Å search boxes. The results of these docking calculations are summarized in Figure 6.

For ZINC13407541, the best score is obtained from docking to center 7 from cluster A (Figure 6a). This site corresponds to the same site that was predicted to bind ZINC13407541 in the original virtual screening campaign (Figure 6b). It is noteworthy that this potential binding site identified by FTMap does not coincide with any other higher-order sites from FTMap. A previous study has recommended the use of only the top five FTMap predicted binding sites for drug design because the lower-order sites overlap with the top five predicted centers.[106] However, in the present case, we decided to use all FTMap sites in order to search as much of the protein surface as possible. Indeed, we found that the best-scoring pose would not have been found if only the top five sites had been used.

Next, we examined a subset of the docking results of ZINC13407541 in which all of the best-scoring poses were within the error of the single, best-scoring pose over all possible binding sites identified by FTMap. The error here is taken to be the standard deviation over all the docking simulations performed in the MED search. Fifteen docking poses resulted, 12 of which were located in the predicted FGF23:FGFR interface[37] (Figure 6a,b) although the best-scoring pose does not correspond to the region of FGF23 predicted to interact with FGFR. Hence, while the multicenter ensemble docking reproduced the result of the original screening campaign, this additional analysis suggests that it indeed might be possible for ZINC13407541 to bind the area predicted to form FGF23:FGFR interactions, which the original campaign predicted only for ZINC01626100.

ZINC01626100 was also docked to the same possible binding sites identified by FTMap. Ten poses were selected for this molecule, using the same procedure as ZINC13407541. Nine of the poses were found to be at the predicted protein–protein interface. The best-scoring pose for ZINC01626100 was found to be in center 1 of cluster B (Figure 6c,d). This finding is again consistent with the result of the original screening campaign. The pocket identified for ZINC13407541 that is not located at the predicted protein–protein interface was not found for ZINC01626100 even though the same FTMap centers were used (Figure 6). This result suggests the possibility that there is a unique binding pocket for each antagonist molecule.

The conclusions drawn from the above analysis, which incorporates the error of the data set, are that the possibility exists that ZINC13407541 might bind to the same region as ZINC01626100, with both molecules disrupting protein–protein interactions between FGF23 and FGFR. However, the results do not discount the possibility of a unique pocket for ZINC13407541.

MM/PBSA rescoring suggests that the preferred binding mode of ZINC13407541 is at the predicted FGF23:FGFR interface

To obtain more accurate predictions of the binding sites and poses of ZINC13407541 on FGF23, and in an effort to discriminate between the two possibilities shown in the MED for this compound, the MM/PBSA method was used to estimate the binding free energy of ZINC13407541 to the set of docking poses determined in the MED and described above. Short MD simulations were performed to sample the configurational space in the immediate vicinity of the docking results. The use of an all-atom MD force field also explicitly takes into account conformational energies that are neglected in the AutoDock scoring function such as dihedral angles.

The results suggest that the most favorable binding affinity is within the FGF23:FGFR interface and not the distal pocket identified in the initial virtual screen of the refined homology models (Figure 7). The binding area corresponding to cluster B, center 2 (Figure 6a) has the most favorable estimated binding free energy upon MM/PBSA rescoring (Figure 7E). The weakest predicted binding pocket examined was also located within the FGF23:FGFR interface (Figure 7J). This peculiar finding warranted further examination. There are two possible reasons for this result. Either the choice of the center of the docking box precluded ligand binding at the best-rescored site, or the protein conformation prevented the molecule from finding the best pose. Further investigation revealed that the size and position of the docking box were sufficient to find the proper pose, but side-chain conformations in the snapshot used blocked the pocket (Figure 7c). This observation highlights the importance of snapshot selection in docking and further reiterates the need to incorporate extensive side-chain variability in docking studies.

MM/PBSA appears to discriminate between different sites and poses obtained in the MED search. Indeed, others have used MM/GBSA to rerank compounds from in silico screening with success.[23] In the present study, we have used MM/PBSA to discriminate between possible binding pockets, as a first step toward rational lead optimization of FGF23 antagonist compounds and to predict possible binding sites that can be tested experimentally.

Protein–protein docking suggests that the binding region found by MED of FGF23 forms interactions with FGFR1

It is useful to conduct an independent computational test of whether or not the areas found by MED of FGF23 and the initial high-throughput in silico screen are indeed areas that can form protein–protein interactions with FGFR. To this end, protein–protein docking of FGF23 and FGFR1 was conducted, in which the FGF23 crystal structure was docked as the ligand, and FGFR1 was used as the receptor, with the ClusPro web server.[94,95,107] FGFR1 has been shown to form a functional receptor complex with FGF23.[108] The existence of a crystal structure in which FGFR1 is cocrystallized with FGF2[109] makes this FGFR a good choice for protein–protein docking with FGF23.

ClusPro[94,95] has been shown to identify native protein complex structures and is therefore a good choice for the current study.[110] The scoring function used by ClusPro can be weighted toward electrostatic interactions, hydrophobic interactions, a combined van der Waals/electrostatics weighting, or a set of balanced weights for all contributions.

The top ten models for each predefined set of scoring function weights are summarized in Table S1. Of the top ten poses predicted with the balanced scoring function, six found the protein–protein contacts predicted by Yamazaki et al.[37] For the form of the scoring function that is

weighted toward electrostatics, seven of the top ten models found these areas. In the docked complexes that were weighted toward the hydrophobic term, eight of the top ten models found the protein–protein contacts. In contrast, the weighting of the van der Waals and electrostatic terms over the shape complementarity term produced models for which only the top two found the previously predicted regions of protein–protein contacts.

It is interesting that a majority of the models have the same protein–protein contacts previously predicted on the basis of a sequence alignment of FGF23 with FGF2.[37] These findings support the hypothesis that disrupting FGF23-FGFR interactions is a mechanism for FGF23 inhibition. Some of these models are shown in Figure 8. The interplay between the error in the protein–protein docking simulations and the weights of the different scoring functions will be addressed in a future study.

Conclusions

The work presented herein describes an ensemble approach to the interpretation of docking results for a target for which there is only a partial crystal structure and no a priori knowledge of small-molecule binding sites. We have used a multicenter ensemble docking approach to identify two possible binding regions for drug-like antagonist compounds binding to the hormone FGF23. If a static, single-point approach had been used, the possibility of ZINC13407541 also binding the predicted protein–protein interface would have been missed. The further refinement of the MED results with MM/PBSA rescoring highlights the usefulness of moving from lower-resolution techniques to higher-resolution methods for refinement of a predicted binding mode. The current study also shows how snapshot selection can influence docking results through the steric crowding of pockets by side-chain conformers.

It is important to view the current work in the environment in which it is most likely to be applied. In drug discovery settings, particularly computationally lead drug discovery such as the present work, the role of the computational chemist is to formulate hypothesis through simulation about how a protein target can be drugged. In the virtual screening part of this study, predictions are made about what drug-like compounds from a compound library are likely to antagonize FGF23 signaling. These predictions are verified in the work of Xiao et al.[49] where target engagement studies, mouse model experimentation, and co-immunoprecipitation experiments indicate that these compounds not only antagonize FGF23 signaling, but that one of the compounds, ZINC13407541, has therapeutic potential to treat hypophosphatemia. The MED, MM/PBSA, and protein–protein docking parts of this study develop a hypothesis where a mechanism of action for the antagonist compounds can be further explored through experiment. It is noteworthy that the hypothesis developed in this work indicates that a protein–protein interface is being drugged and not a distal pocket that would indicate allosteric signaling. This is consistent with previous experimental evidence.[37,49]

Protein–protein interfaces are difficult targets to drug because they tend to consist of multiple shallow pockets instead of a single deep pocket.111] These difficulties have led to the use of peptidomimetics and engineered antibodies instead of small-molecule modulators. However, antibodies and peptidomimetics are expensive to produce, have lower bioavailability, and generally suffer from problems with cell permeability.[112] In the future, protocols similar to that presented here may be of general applicability in targeting protein–protein interfaces, and, more generally, for difficult protein targets for which structural information is lacking.

References

[1] J. H. Van Drie, *J. Comput. Aided Mol. Des.* **2007**, *21*, 591.

[2] C. M. Song, S. J. Lim, J. C. Tong, *Brief. Bioinform.* **2009**, *10*, 579.

[3] R. Lahana, *Drug Discov. Today* **1999**, *4*, 447.

[4] D. R. Houston, L.-H. Yen, S. Pettit, M. D. Walkinshaw, *PLoS ONE* **2015**, *10* (4), e0121424.

[5] K. Siddiquee, S. Zhang, W. C. Guida, M. A. Blaskovich, B. Greedy, H. R. Lawrence, M. R. Yip, R. Jove, M. M. McLaughlin, N. J. Lawrence, *Proc. Natl Acad. Sci.* **2007**, *104*, 7391.

[6] C. de Graaf, A. J. Kooistra, H. F. Vischer, V. Katritch, M. Kuijer, M. Shiroishi, S. Iwata, T. Shimamura, R. C. Stevens, I. J. P. de Esch, R. Leurs, *J. Med. Chem.* **2011**, *54*, 8195.

[7] H. A. Carlson, *Curr. Opin. Chem. Biol.* **2002**, *6*, 447.

[8] P. Cozzini, G. E. Kellogg, F. Spyrakis, D. J. Abraham, G. Costantino, A. Emerson, F. Fanelli, H. Gohlke, L. A. Kuhn, G. M. Morris, M. Orozco, T. A. Pertinhez, M. Rizzi, C. A. Sotriffer, *J. Med. Chem.* **2008**, *51*, 6237.

[9] S. L. McGovern, B. K. Shoichet, *J. Med. Chem.* **2003**, *46*, 2895.

[10] S. R. Ellingson, Y. Miao, J. Baudry, J. C. Smith, *J. Phys. Chem. B* **1026**, *2015*, 119.

[11] W. Evangelista, R. L. Weir, S. R. Ellingson, J. B. Harris, K. Kapoor, J. C. Smith, J. Baudry, *Bioorg. Med. Chem.* **2016**, *24*, 4928.

[12] R. E. Amaro, A. Schnaufer, H. Interthal, W. Hol, K. D. Stuart, J. A. McCammon, *Proc. Natl Acad. Sci. USA* **2008**, *105*, 17278.

[13] C. W. Murray, C. A. Baxter, A. D. Frenkel, *J. Comput. Aided Mol. Des.* **1999**, *13*, 547.

[14] S.-Y. Huang, X. Zou, *Proteins: Struct. Funct. Bioinf.* **2007**, *66*, 399.

[15] N. Foloppe, I. J. Chen, *Bioorg. Med. Chem.* **2016**, *24*, 2159.

[16] D. S. Goodsell, A. J. Olson, *Proteins: Struct. Funct. Bioinf.* **1990**, *8*, 195.

[17] T. N. Hart, R. J. Read, *Proteins: Struct. Funct. Bioinf.* **1992**, *13*, 206.

[18] R. S. Judson, E. P. Jaeger, A. M. Treasurywala, *J. Mol. Struct. (Thoechem)* **1994**, *308*, 191.

[19] R. M. Jackson, *J. Comput. Aided Mol. Des.* **2002**, *16*(1), 43.

[20] C. A. Baxter, C. W. Murray, D. E. Clark, D. R. Westhead, M. D. Eldridge, *Proteins: Struct. Funct. Bioinf.* **1998**, *33*, 367.

[21] D. Plewczynski, M. Łaźniewski, R. Augustyniak, K. Ginalski, *J. Comput. Chem.* **2011**, *32*, 742.

[22] M. Feher, C. I. Williams, *J. Chem. Inf. Model.* **2012**, *52*, 724.

[23] P. A. Greenidge, C. Kramer, J. C. Mozziconacci, W. Sherman, *J. Chem. Inf. Model.* **2014**, *54*, 2697.

[24] I. R. Craig, J. W. Essex, K. Spiegel, *J. Chem. Inf. Model.* **2010**, *50*, 511.

[25] S.-Y. Huang, X. Zou, *Protein Sci.* **2007**, *16*(1), 43.

[26] E. M. Novoa, L. R. D. Pouplana, X. Barril, M. Orozco, *J. Chem. Theory Comput.* **2010**, *6*, 2547.

[27] K. Kapoor, N. McGill, C. B. Peterson, H. V. Meyers, M. N. Blackburn, J. Y. Baudry, *J. Chem. Inf. Model.* **2016**, *6*, 2457.

[28] Z. X. Xiang, *Curr. Protein Pept. Sci.* **2006**, *7*, 217.

[29] M. Mangoni, D. Roccatano, A. Di Nola, *Proteins: Struct. Funct. Bioinf.* **1999**, *35*, 153.

[30] B. Huang, M. Schroeder, *BMC Struct. Biol.* **2006**, *6*(1), 1.

[31] O. Guvench, A. D. MacKerell Jr., *PLoS Comput. Biol.* **2009**, *5*(7), e1000435.

[32] R. Brenke, D. Kozakov, G.-Y. Chuang, D. Beglov, D. Hall, M. R. Landon, C. Mattos, S. Vajda, *Bioinformatics* **2009**, *25*, 621.

[33] D. Kozakov, L. E. Grove, D. R. Hall, T. Bohnuud, S. E. Mottarella, L. Luo, B. Xia, D. Beglov, S. Vajda, *Nat. Protocols* **2015**, *10*, 733.

[34] N. Burgoyne, R. Jackson, *Bioinformatics* **2006**, *22*, 733.

[35] R. Goetz, A. Beenken, O. A. Ibrahimi, J. Kalinina, S. K. Olsen, A. V. Eliseenkova, C. Xu, T. A. Neubert, F. Zhang, R. J. Linhardt, X. Yu, K. E. White, T. Inagaki, S. A. Kliewer, M. Yamamoto, H. Kurosu, Y. Ogawa, M. Kuro-o, B. Lanske, M. S. Razzaque, M. Mohammadi, *Mol. Cell. Biol.* **2007**, *27*, 3417.

[36] I. Urakawa, Y. Yamazaki, T. Shimada, K. Iijima, H. Hasegawa, K. Okawa, T. Fujita, S. Fukumoto, T. Yamashita, *Nature* **2006**, *444*, 770.

[37] Y. Yamazaki, T. Tamada, N. Kasai, I. Urakawa, Y. Aono, H. Hasegawa, T. Fujita, R. Kuroki, T. Yamashita, S. Fukumoto, T. Shimada, *J. Bone Miner. Res.* **2008**, *23*, 1509.

[38] L. D. Quarles, *Nat. Med.* **2011**, *17*, 428.

[39] T. Shimada, T. Muto, I. Urakawa, T. Yoneya, Y. Yamazaki, K. Okawa, Y. Takeuchi, T. Fujita, S. Fukumoto, T. Yamashita, *Endocrinology* **2002**, *143*, 3179.

[40] X. Bai, D. Miao, J. Li, D. Goltzman, A. C. Karaplis, *Endocrinology* **2004**, *145*, 5269.

[41] L. D. Quarles, *Nat. Rev. Endocrinol.* **2012**, *8*, 276.

[42] H. Komaba, M. Fukagawa, *Kidney Int.* **2009**, *77*, 292.

[43] L. Craver, M. P. Marco, I. Martinez, M. Rue, M. Borras, M. L. Martin, F. Sarro, J. M. Valdivielso, E. Fernandez, *Nephrol. Dial. Transplant.* **2007**, *22*, 1171.

[44] O. M. Gutierrez, M. Mannstadt, T. Isakova, J. A. Rauh-Hain, H. Tamez, A. Shah, K. Smith, H. Lee, R. Thadhani, H. Juppner, M. Wolf, *N. Engl. J. Med.* **2008**, *359*, 584.

[45] D. Fliser, B. Kollerits, U. Neyer, D. P. Ankerst, K. Lhotta, A. Lingenhel, E. Ritz, F. Kronenberg, *J. Am. Soc. Nephrol.* **2007**, *18*, 2600.

[46] M. A. I. Mirza, J. Alsio, A. Hammarstedt, R. G. Erben, K. Michaelsson, A. Tivesten, R. Marsell, E. Orwoll, M. K. Karlsson, O. Ljunggren, D. Mellstrom, L. Lind, C. Ohlsson, T. E. Larsson, *Arterioscler. Thromb. Vasc. Biol.* **2011**, *31*, 219.

[47] I. Z. Ben-Dov, H. Galitzer, V. Lavi-Moshayoff, R. Goetz, M. Kuro-o, M. Mohammadi, R. Sirkis, T. Naveh-Many, J. Silver, *J. Clin. Investig.* **2007**, *117*, 4003.

[48] S. Fukumoto, T. Yamashita, *Curr. Opin. Nephrol. Hypertens.* **2002**, *11*, 385.

[49] Z. Xiao, D. Riccardi, H. A. Velazquez, A. L. Chin, C. R. Yates, J. D. Carrick, J. C. Smith, J. Baudry, L. D. Quarles, *Sci. Signal.* **2016**, *9*, ra113.

[50] H. A. Carlson, J. A. McCammon, *Mol. Pharmacol.* **2000**, *57*, 213.

[51] B. J. Grant, S. Lukman, H. J. Hocker, J. Sayyah, J. H. Brown, J. A. McCammon, A. A. Gorfe, *PLoS ONE* **2011**, *6*(10), e25711.

[52] J.-H. Lin, A. L. Perryman, J. R. Schames, J. A. McCammon, *J. Am. Chem. Soc.* **2002**, *124*, 5632.

[53] J. A. McCammon, *Biochim. Biophys. Acta* **2005**, *1754*, 221.

[54] Y. Miao, S. E. Nichols, J. A. McCammon, *Chem. Biol. Drug Des.* **2014**, *83*, 237.

[55] O. Trott, A. J. Olson, *J. Comput. Chem.* **2010**, *31*, 455.

[56] C. A. Lipinski, *Drug Discov. Today: Technol.* **2004**, *1*, 337.

[57] C. A. Lipinski, *J. Pharmacol. Toxicol. Methods* **2000**, *44*, 35.

[58] D. F. Veber, S. R. Johnson, H.-Y. Cheng, B. R. Smith, K. W. Ward, K. D. Kopple, *J. Med. Chem.* **2002**, *45*, 2615.

[59] W. P. Walters, M. A. Murcko, *Adv. Drug Deliv. Rev.* **2002**, *54*, 255.

[60] C. A. Lipinski, F. Lombardo, B. W. Dominy, P. J. Feeney, *Adv. Drug Deliv. Rev.* **2001**, *46*(1–3), 3.

[61] A. K. Ghose, V. N. Viswanadhan, J. J. Wendoloski, *J. Comb. Chem.* **1999**, *1*(1), 55.

[62] I. Muegge, *Chem. Eur. J.* **1976**, *2002*, 8.

[63] A. Biegert, C. Mayer, M. Remmert, J. Soding, A. N. Lupas, *Nucleic Acids Res.* **2006**, *34*(suppl 2), W335.

[64] J. Soding, A. Biegert, A. N. Lupas, *Nucleic Acids Res.* **2005**, *33*(Web Server issue), W244.

[65] N. J. Harmer, L. Pellegrini, D. Chirgadze, J. Fernandez-Recio, T. L. Blundell, *Biochemistry* **2004**, *43*, 629.

[66] S. K. Olsen, M. Garbi, N. Zampieri, A. V. Eliseenkova, D. M. Ornitz, M. Goldfarb, M. Mohammadi, *J. Biol. Chem.* **2003**, *278*, 34226.

[67] N. Eswar, B. Webb, M. A. Marti-Renom, M. S. Madhusudhan, D. Eramian, M.-Y. Shen, U. Pieper, A. Sali, Comparative Protein Structure Modeling Using Modeller, John Wiley & Sons Inc, In Current Protocols in Bioinformatics **2002**.

[68] S. Jo, T. Kim, V. G. Iyer, W. Im, *J. Comput. Chem.* **1859**, *2008*, 29.

[69] B. R. Brooks, C. L. Brooks, A. D. Mackerell, L. Nilsson, R. J. Petrella, B. Roux, Y. Won, G. Archontis, C. Bartels, S. Boresch, A. Caflisch, L. Caves, Q. Cui, A. R. Dinner, M. Feig, S. Fischer, J. Gao, M. Hodoscek, W. Im, K. Kuczera, T. Lazaridis, J. Ma, V. Ovchinnikov, E. Paci, R. W. Pastor, C. B. Post, J. Z. Pu, M. Schaefer, B. Tidor, R. M. Venable, H. L. Woodcock, X. Wu, W. Yang, D. M. York, M. Karplus, *J. Comput. Chem.* **2009**, *30*, 1545.

[70] A. T. Brunger, M. Karplus, *Proteins: Struct. Funct. Bioinf.* **1988**, *4*, 148.

[71] G. Arfken, Mathematical Methods for Physicists. Elsevier, Waltham **1985**, 428.

[72] J.-W. Chu, B. L. Trout, B. R. Brooks, *J. Chem. Phys.* **2003**, *119*, 12708.

[73] J.-P. Ryckaert, G. Ciccotti, H. J. C. Berendsen, *J. Comput. Phys.* **1977**, *23*, 327.

[74] D. Riccardi, J. M. Parks, A. Johs, J. C. Smith, *J. Chem. Inf. Model.* **2015**, *55*, 721.

[75] J. J. Irwin, B. K. Shoichet, *J. Chem. Inf. Model.* **2005**, *45*, 177.

[76] J. H. Voigt, B. Bienfait, S. Wang, M. C. Nicklaus, *J. Chem. Inf. Comput. Sci.* **2001**, *41*, 702.

[77] T. Tanimoto, An Elementary Mathematical Theory of Classification and Prediction, IBM Report (November, 1958), cited in: G. Salton, Automatic Information Organization and Retrieval, McGraw-Hill, New York **1968**.

[78] X. Chen, C. H. Reynolds, *J. Chem. Inf. Comput. Sci.* **2002**, *42*, 1407.

[79] D. Bajusz, A. Racz, K. Heberger, *J. Cheminform.* **2015**, *7*(1), 1.

[80] N. M. OLBoyle, M. Banck, C. A. James, C. Morley, T. Vandermeersch, G. R. Hutchison, *J. Cheminform.* **2011**, *3*, 33.

[81] N. M. O'Boyle, *J. Cheminform.* **2012**, *4*, 22.

[82] M. F. Sanner, *J. Mol. Graph. Model.* **1999**, *17*(1), 57.

[83] W. L. Jorgensen, J. Chandrasekhar, J. D. Madura, R. W. Impey, M. L. Klein, *J. Chem. Phys.* **1983**, *79*, 926.

[84] V. Hornak, R. Abel, A. Okur, B. Strockbine, A. Roitberg, C. Simmerling, *Proteins: Struct. Funct. Bioinf.* **2006**, *65*, 712.

[85] W. D. Cornell, P. Cieplak, C. I. Bayly, I. R. Gould, K. M. Merz, D. M. Ferguson, D. C. Spellmeyer, T. Fox, J. W. Caldwell, P. A. Kollman, *J. Am. Chem. Soc.* **1995**, *117*, 5179.

[86] J. Huang, A. D. MacKerell, *J. Comput. Chem.* **2013**, *34*, 2135.

[87] J. A. Maier, C. Martinez, K. Kasavajhala, L. Wickstrom, K. E. Hauser, C. Simmerling, *J. Chem. Theory Comput.* **2015**, *11*, 3696.

[88] M. R. Hestenes, E. Stiefel, Methods of Conjugate Gradients for Solving Linear Systems, Springer, New York **1952**.

[89] D. Case, T. Darden, T. E. Cheatham III, C. Simmerling, J. Wang, R. Duke, R. Luo, R. Walker, W. Zhang, K. Merz, AMBER 12. University of California, San Francisco **2012**, 1(3).

[90] D. Kozakov, L. E. Grove, D. R. Hall, T. Bohnuud, S. E. Mottarella, L. Luo, B. Xia, D. Beglov, S. Vajda, *Nat. Protoc.* **2015**, *10*, 733.

[91] C. H. Ngan, T. Bohnuud, S. E. Mottarella, D. Beglov, E. A. Villar, D. R. Hall, D. Kozakov, S. Vajda, *Nucleic Acids Res.* **2012**, *40*(Web Server issue), W271.

[92] C. Lee, W. Yang, R. G. Parr, *Phys. Rev. B* **1988**, *37*, 785.

[93] M. J. Frisch, G. W. Trucks, H. B. Schlegel, G. E. Scuseria, M. A. Robb, J. R. Cheeseman, G. Scalmani, V. Barone, B. Mennucci, G. A. Petersson, H. Nakatsuji, M. Caricato, X. Li, H. P. Hratchian, A. F. Izmaylov, J. Bloino, G. Zheng, J. L. Sonnenberg, M. Hada, M. Ehara, K. Toyota, R. Fukuda, J. Hasegawa, M. Ishida, T. Nakajima, Y. Honda, O. Kitao, H. Nakai, T. Vreven, J. A. Montgomery Jr, J. E. Peralta, F. Ogliaro, M. J. Bearpark, J. Heyd, E. N.

Brothers, K. N. Kudin, V. N. Staroverov, R. Kobayashi, J. Normand, K. Raghavachari, A. P. Rendell, J. C. Burant, S. S. Iyengar, J. Tomasi, M. Cossi, N. Rega, N. J. Millam, M. Klene, J. E. Knox, J. B. Cross, V. Bakken, C. Adamo, J. Jaramillo, R. Gomperts, R. E. Stratmann, O. Yazyev, A. J. Austin, R. Cammi, C. Pomelli, J. W. Ochterski, R. L. Martin, K. Morokuma, V. G. Zakrzewski, G. A. Voth, P. Salvador, J. J. Dannenberg, S. Dapprich, A. D. Daniels, O. Farkas, J. B. Foresman, J. V. Ortiz, J. Cioslowski, D. J. Fox, Gaussian 09, Gaussian Inc., Wallingford, CT, USA **2009**.

[94] S. R. Comeau, D. W. Gatchell, S. Vajda, C. J. Camacho, *Bioinformatics* **2004**, *20*(1), 45.

[95] S. R. Comeau, D. W. Gatchell, S. Vajda, C. J. Camacho, *Nucleic Acids Res.* **2004**, *32*(suppl 2), W96.

[96] J. J. Ward, L. J. McGuffin, K. Bryson, B. F. Buxton, D. T. Jones, *Bioinformatics* **2004**, *20*, 2138.

[97] D. T. Jones, D. Cozzetto, *Bioinformatics* **2015**, *31*, 857.

[98] A. Raval, S. Piana, M. P. Eastwood, R. O. Dror, D. E. Shaw, *Proteins: Struct. Funct. Bioinf.* **2012**, *80*, 2071.

[99] Y. Pan, N. Huang, S. Cho, A. D. MacKerell, *J. Chem. Inf. Comput. Sci.* **2003**, *43*, 267.

[100] G. Carta, A. J. S. Knox, D. G. Lloyd, *J. Chem. Inf. Model.* **2007**, *47*, 1564.

[101] C. K. Kirtay, J. B. O. Mitchell, J. A. Lumley, *QSAR Comb. Sci.* **2005**, *24*, 527.

[102] H. Clausen, C. Buning, M. Rarey, T. Lengauer, *J. Mol. Biol.* **2001**, *308*, 377.

[103] S. Tian, H. Sun, P. Pan, D. Li, X. Zhen, Y. Li, T. Hou, *J. Chem. Inf. Model.* **2014**, *54*, 2664.

[104] A. Ivetac, J. Andrew McCammon, *Chem. Biol. Drug Des.* **2010**, *76*, 201.

[105] J. M. Ortiz-Sanchez, S. E. Nichols, J. Sayyah, J. H. Brown, J. A. McCammon, B. J. Grant, *PLoS ONE* **2012**, *7*(7), e40809.

[106] D. R. Hall, C. H. Ngan, B. S. Zerbe, D. Kozakov, S. Vajda, *J. Chem. Inf. Model.* **2012**, *52*, 199.

[107] D. Kozakov, R. Brenke, S. R. Comeau, S. Vajda, *Proteins: Struct. Funct. Bioinf.* **2006**, *65*, 392.

[108] X. Zhang, O. A. Ibrahimi, S. K. Olsen, H. Umemori, M. Mohammadi, D. M. Ornitz, *J. Biol. Chem.* **2006**, *281*, 15694.

[109] J. Schlessinger, A. N. Plotnikov, O. A. Ibrahimi, A. V. Eliseenkova, B. K. Yeh, A. Yayon, R. J. Linhardt, M. Mohammadi, *Mol. Cell* **2000**, *6*, 743.

[110] D. Kozakov, D. Beglov, T. Bohnuud, S. E. Mottarella, B. Xia, D. R. Hall, S. Vajda, *Proteins: Struct. Funct. Bioinf.* **2013**, *81*, 2159.

[111] P. Fischer, *Drug Design Rev. Online* **2005**, *2*, 179.

[112] N. Qvit, J. A. Crapster, *Chimica Oggi/CHEMISTRY Today* **2014**, *32*(6), 31.

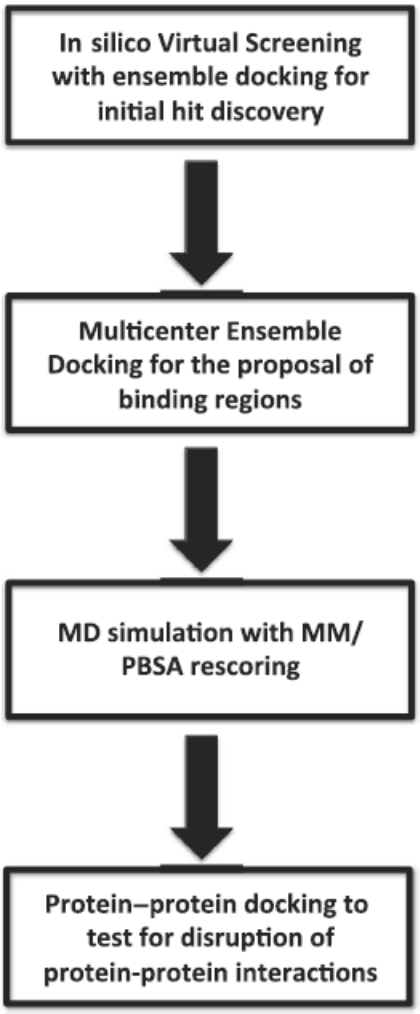

Scheme 1: Workflow that resulted in the trial compounds that were experimentally verified in Xiao et al. along with the refinements that lead to the hypothesis that the antagonist molecules are disrupting protein–protein interactions between FGF23 and FGFR.

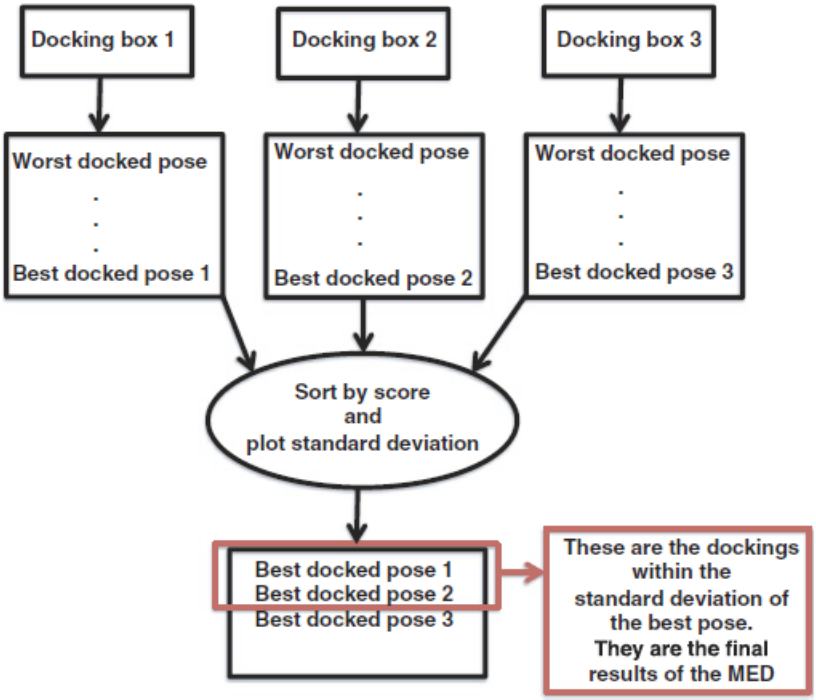

Scheme 2: Flowchart for the analysis of the multicenter ensemble docking (MED) simulations. This procedure was followed for each FGF23 structure used to perform the MED.

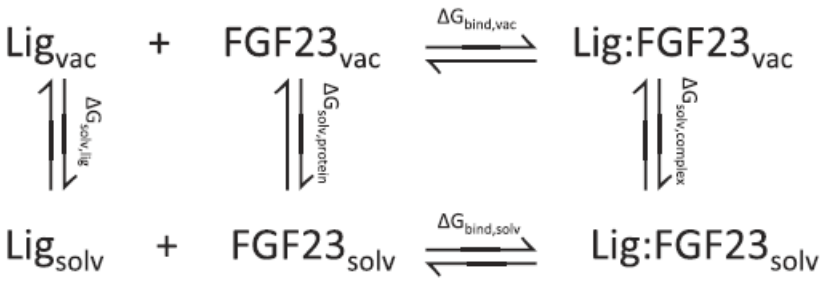

Scheme 3: Thermodynamic cycle of protein–ligand binding used to estimate binding free energies with the MM/PBSA method.

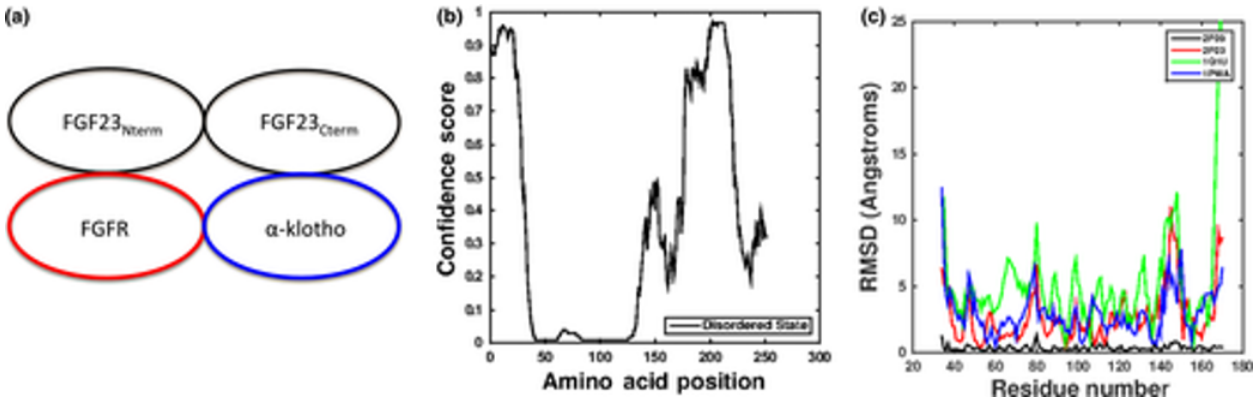

Figure 1. (a) FGF23 interacting with its binary receptor complex in the orientation proposed by Yamazaki et al. where the N-terminal fragment of FGF23 interacts with FGFR and the C-terminal fragment interacts with alpha-klotho. (b) Intrinsic disorder profile of FGF23 from disopred3. (c) Residue–residue pairwise RMSD of the alpha carbons along the backbone of the refined homology models versus the FGF23 X-ray structure (PDB ID: 2P39).

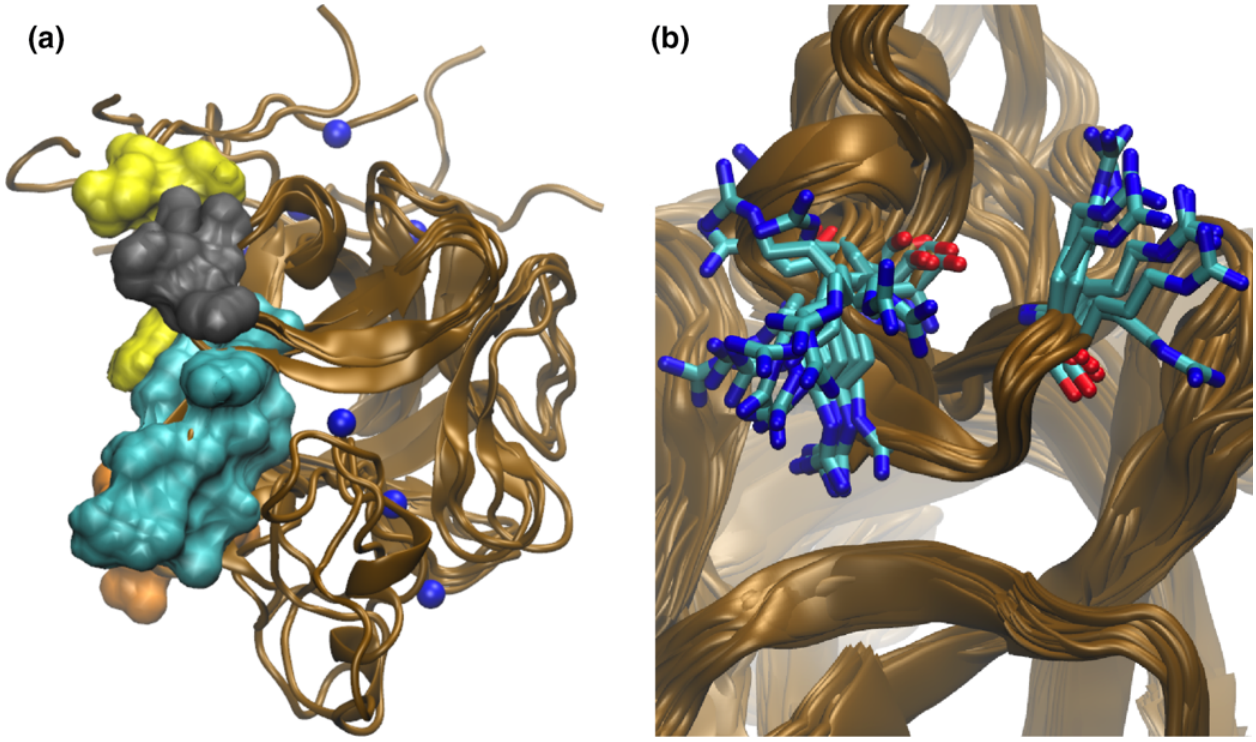

Figure 2. (a) Refined FGF23 models with possible binding sites (spheres) that were used as the center of search boxes in the in silico screening campaign. The areas predicted to form protein–protein interactions with FGFR are shown in cyan, orange, yellow, and gray surf. (b) Side-chain variability captured in the ensemble of Arg140.

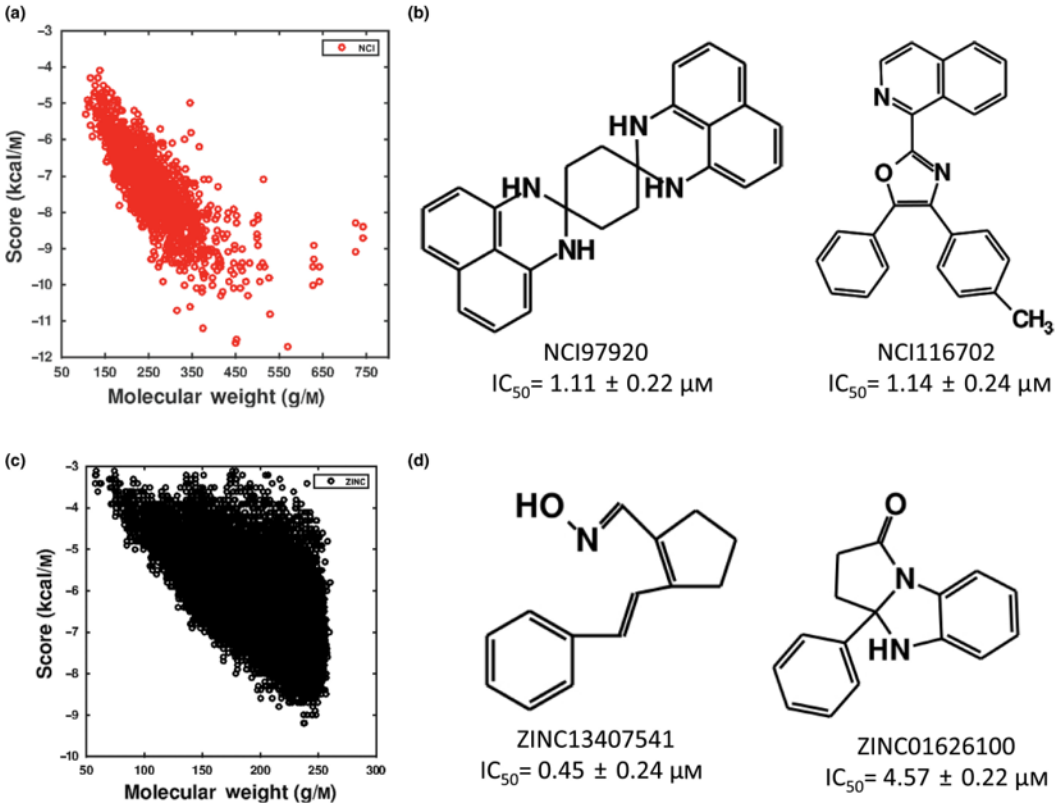

Figure 3. (a) In silico docking screen of the NCI diversity set 2. (b) Trial compounds from the NCI screen that were verified to be FGF23 antagonist in Xiao et al. with their IC_{50} values. Experimentally verified FGF23 inhibitors and their IC_{50} values. (c) In silico docking screen of the ZINC Drugs Now subset of the ZINC database. (d) Trial compounds from the ZINC Drugs Now screen that were verified to be FGF23 antagonist in Xiao et al. with their IC_{50} values.

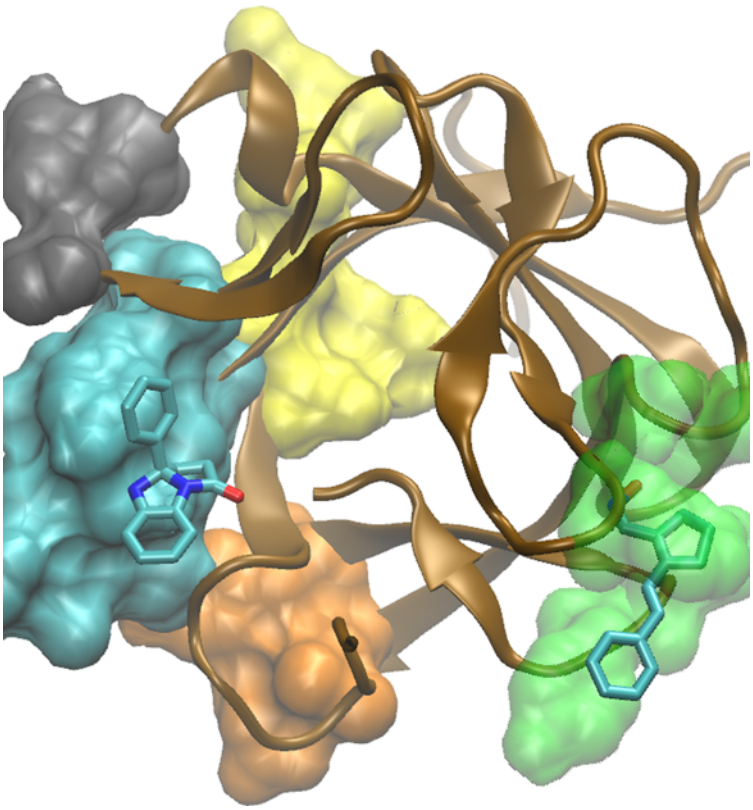

Figure 4. Highest-ranking poses of the FGF23 compounds that performed well on drug-likeness filters from the in silico high-throughput screening campaign. The regions predicted by Yamazaki et al. to form protein–protein interactions with FGFR are colored cyan, orange, gray, and yellow. Hydrogen atoms are omitted on the drug compounds for clarity.

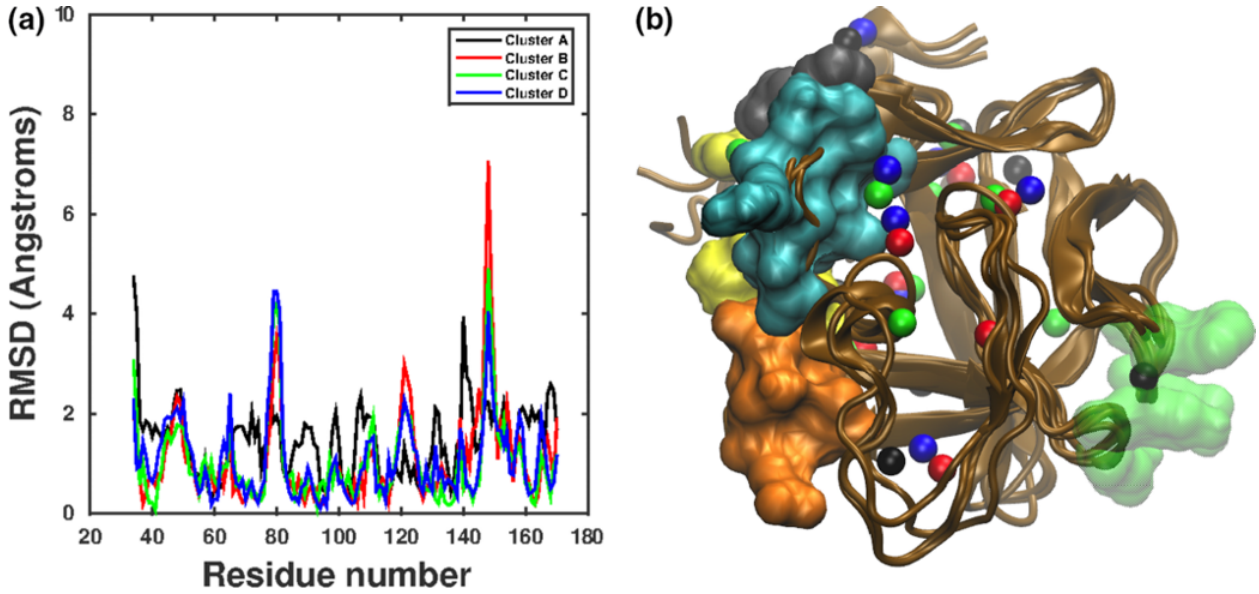

Figure 5. (a) Pairwise RMSD of the alpha carbons along the backbone of the snapshots used for the MED versus the FGF23 X-ray structure (PDB ID: 2P39). (b) Structures derived from conformational cluster analysis of an MD simulation submitted to the FTMap web server for identification of possible binding sites of the FGF23 antagonist molecules. Regions predicted to form interactions with FGFR are colored in orange, cyan, yellow, and gray surface. An FTMap center associated with a possible binding pocket distal to the predicted protein–protein interface is colored in transparent green. The possible binding sites identified by FTMap are shown as spheres. The black spheres correspond to the possible sites found on representative cluster A, red spheres are for cluster B, green spheres are for cluster C, and blue spheres are for cluster D.

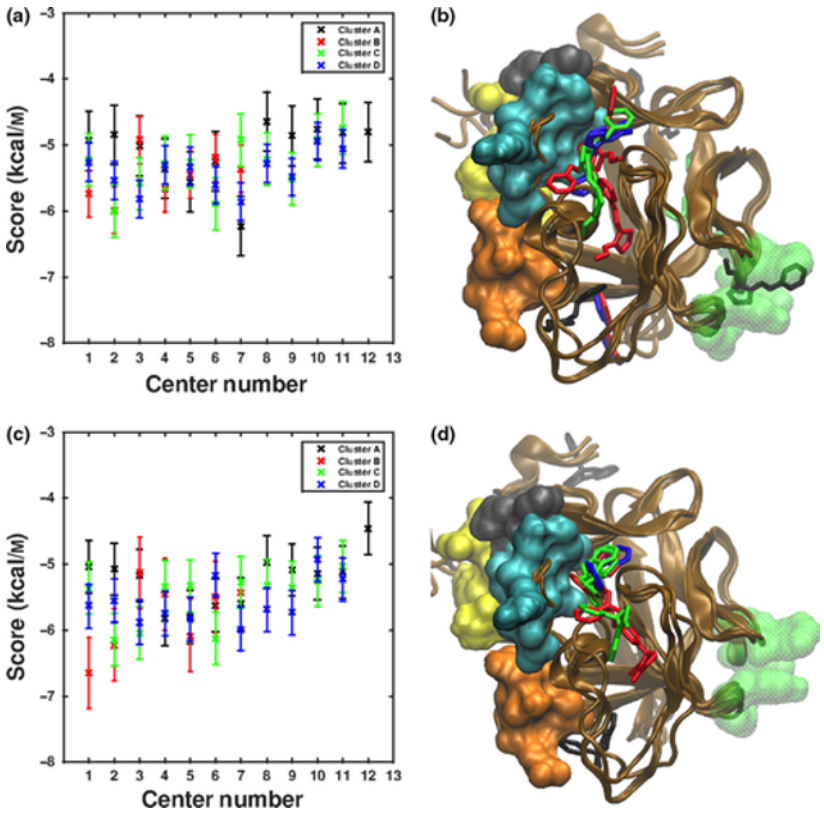

Figure 6. (a) Results of multicenter ensemble docking of ZINC13407541 to $FGF23_{Nterm}$. (b) The subset of 15 docking poses where 12 of the 15 dockings find areas predicted to participate in protein–protein interactions along with the distal pocket for ZINC13407541 in green. (c) Results of multicenter ensemble docking of ZINC01626100 to $FGF23_{Nterm}$. (d) The subset of ten docking poses of ZINC01626100 where nine find the areas predicted to participate in protein–protein interactions with FGFR.

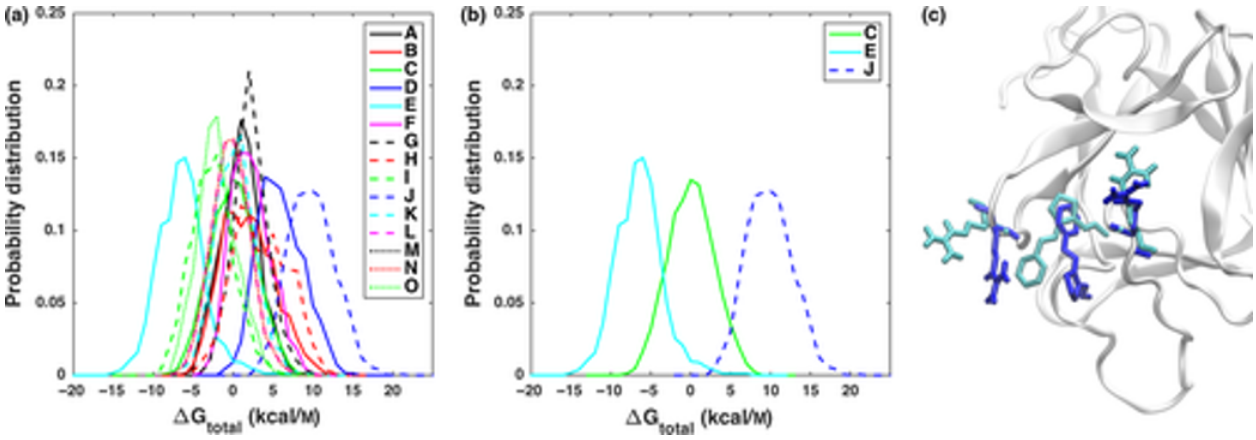

Figure 7. (a) Distributions of the estimated binding affinities from the MM/PBSA for the subset of dockings examined in the MED of ZINC13407541. (b) The distribution of the best binding pocket per the MM/PBSA analysis (cyan), the possible distal pocket for ZINC13407541 (green), and the worst possible pocket (blue dash). E and J correspond to the region where FGF23:FGFR interactions are predicted to form. (c) The best docked pose (cyan) and the corresponding FGF23 side-chain conformations (also in cyan) with the worst ligand pose (blue) with the associated side-chain conformations (also in blue).

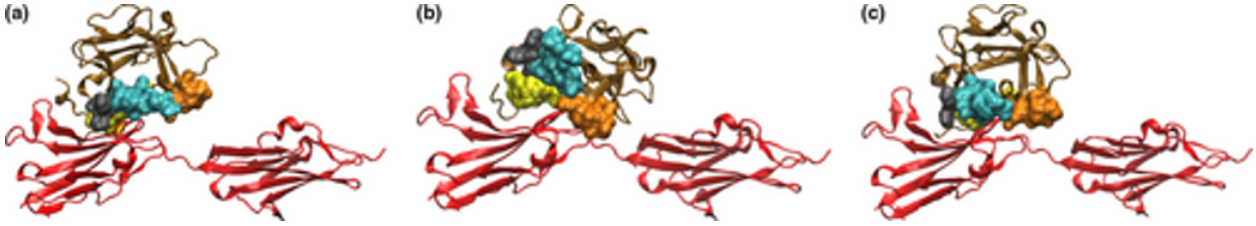

Figure 8. Representative models produced from protein–protein dockings with ClusPro. (a) Model produced from the balanced scoring function. (b) The scoring function weighted for electrostatics and (c) The scoring function for hydrophobic interactions. The regions predicted to participate in protein–protein interactions with FGFR1 are colored in surface as cyan, orange, yellow, and gray.

Table 1. Number of possible pockets identified by FTMap in the refined homology models

Refined Model	**Number of possible sites identified**	**Reduced number of possible sites**
1PWA	12	3
1Q1U	9	2
2P23	10	2
2P39	9	2

Table 2. Number of possible binding sites identified by FTMap for MED analysis

Representative FGF23 snapshot	**Number of consensus of possible sites identified**
A	12
B	7
C	11
D	11